Centrifuge model test of an irrigation-induced loess landslide in the Heifangtai loess platform, Northwest China

CUI Sheng-hua[1] http://orcid.org/0000-0002-6638-230X; e-mail: shenghuacui.geo@gmail.com

PEI Xiang-jun[1]* http://orcid.org/0000-0003-0790-4099; e-mail: peixj0119@tom.com

WU Hao-yu[2] http://orcid.org/0000-0002-3685-074X; e-mail: 232569211 @qq.com

HUANG Run-qiu[1] http://orcid.org/0000-0003-2560-4962; e-mail: hrq@cdut.edu.cn

* Corresponding author

1 State Key Laboratory of Geohazard Prevention and Geoenvironment Protection, Chengdu University of Technology, Chengdu 610059, China

2 Sichuan Provincial Transport Department Highway Planning, Survey, Design and Research Institute, Chengdu 610041, China

Citation: Cui SH, Pei XJ, Wu HY, et al. (2018) Centrifuge model test of an irrigation-induced loess landslide in the Heifangtai loess platform, Northwest China. Journal of Mountain Science 15(1). https://doi.org/10.1007/s11629-017-4490-0

Abstract: The Heifangtai platform in Northwest China is famous for irrigation-induced loess landslides. This study conducted a centrifuge model test with reference to an irrigation-induced loess landslide that occurred in Heifangtai in 2011. The loess slope model was constructed by whittling a cubic loess block obtaining from the landslide site. The irrigation water was simulated by applying continuous infiltration from back of the slope. The deformation, earth pressure, and pore pressure were investigated during test by a series of transducers. For this particular study, the results showed that the failure processes were characterized by retrogressive landslides and cracks. The time dependent reductions of cohesion and internal friction angle at basal layer with increasing pore-water pressure were responsible for these failures. The foot part of slope is very important for slope instability and hazard prevention in the study area, where concentration of earth pressure and generation of high pore-water pressures would form before failures. The measurements of earth pressure and pore-water pressure might be effective for early warning in the study area.

Introduction

Loess with an area of 6.31×10^5 km² represents about 6.6% of the total area of China (Liu 1985). Most of these areas are arid, such as Heifangtai in Gansu Province, Northwest China. Dry loess usually has high cementation strength, and can maintain good stability (Lin and Wang 1988), so earthquakes and excavations become the main factors triggering loess landslide in these regions (Derbyshire et al. 1991; Wang 1992; Lei 2001; Li et al. 2007). However, loess may collapse rapidly with increasing water content (Derbyshire et al. 1994; Meng et al. 1998), which was one of the most common triggers of loess landslides all over the world (Derbyshire et al. 2000; Weidinger et al. 2001; Wang et al. 2004; Xu et al. 2009). Agricultural irrigation is the most important cause of the loess landslides on the platform edge in

Heifangtai (Lei 1995; Derbyshire et al. 2000; Zhang et al. 2009; Xu et al. 2010; Xu et al. 2011). Xu et al. (2012) showed that there was a rapid increase of groundwater table due to irrigation, and they proposed that this increase resulted in more landslides in this area than lateral area. Wang et al. (1993) pointed out that the long term retention of water in loess caused the slope creep deformation and time-dependent reduction of the soil strength. Increasing groundwater table will increase pore water pressure in soil, which might induce static liquefaction and lead to landslides (Crosta and Prisco 1999; Gattinoni and Francani 2009). Irrigation-induced loess landslides are generally characterized by recurrence; i.e., repeated landslides occur at the same site. Xue et al. (2011) calculated the rate of the slope edge retreat in Heifangtai area from 1977 to 2010 based on DEM data. He found that the retreating gradually featured by concave topography formed by old landslides. Although irrigation-induced loess landslides have been widely recognized, most studies were based on laboratory models without field data, such as flume test. It is a typical laboratory approach at a reduced scale, through which data on failure and post-failure can be obtained (Eckersley 1990). Generally, laboratory model tests of landslides are not well feasible because of their limited sizes (Moriwaki et al. 2004). There may be a large difference in stress filed between model and prototype. Full-scale tests are prohibitively expensive (Wakeman et al. 1997), and the results cannot be fully verified because of many uncertainties in the field. Although regressive loess landslides are time-dependent dynamic events, their processes are also difficult to capture in the field.

Centrifuge modeling technique has been used to study landslide under similar stress conditions within relatively small model with increased acceleration field. Based on the approach, Schofield (1980), Viswanadham and Rajesh (2009), Lee et al. (2008) and Ling et al. (2009) investigated soil slopes instability with various slope angles, heights and groundwater flow conditions. In addition, rainfall-induced soil landslides have been wieldy studied by centrifuge tests (Take and Bolton 2002; Take et al. 2004; Wang et al. 2010). In particular the work of Take et al. (2004), the centrifuge model configuration was consisted in a layered shallow deposit 33° inclined over fixed bedrock. The deposit was composed of two layers, of which the permeability was differences; i.e., the coarser layer soils were more permeable than the upper ones. Their model also imposed hydraulic boundary conditions by consisting in a seepage water line source at the upper right corner of the model. The scale factor equal to 30 was used. Take et al. (2004) detected that transient localized pore-water pressures originating from the combination of particular hydraulic boundary conditions and stratigraphically settings would result in slope local failures. This mechanism producing a variation in the slope geometry cased the transition of slope post-failure from slide to flow. And static liquefaction would be likely to occur with the increase of pore-water pressures if soil was saturated. Later, the centrifuge model of Take et al. (2004) was employed by Cascini et al (2013) for their simulation study. Centrifuge approach also have been used for other triggering factors that differ from rainfall, such as excavation (Tamrakar et al. 2006; Toyosawa et al. 1996) and earthquake (Zhang et al. 2016; Thusyanthan et al. 2007; Yu et al. 2008; Wang and Zhang 2014), but the studies of irrigation-induced loess landslides are limited.

In this study, a typical irrigation-induced loess landslide (13th Jiaojiayatou landslide) that occurred in 2011 on the edge of the Heifangtai loess platform was chosen for our centrifuge modeling test. A design for simulating irrigation in the centrifuge test was used. The deformation, pore water pressure and earth pressure were measured during the test. The failure processes and mechanism of irrigation-induced loess landslides were studied.

1 Case History

The Heifangtai loess platform is located in 42 km west of Lanzhou City, Gansu Province (Figure 1a). In this region, the average annual rainfall is 287 mm while the annual evaporation is as high as 1593 mm (Xu et al. 2011) (Figure 2a). In order to feed the vast population, the Heifangtai platform has been converted to farmland since the 1950s resulting in extensive irrigation. From 2007 to 2010, the annual irrigation volume in this area increased from 496×10^4 m³ to 609×10^4 m³ (Wang
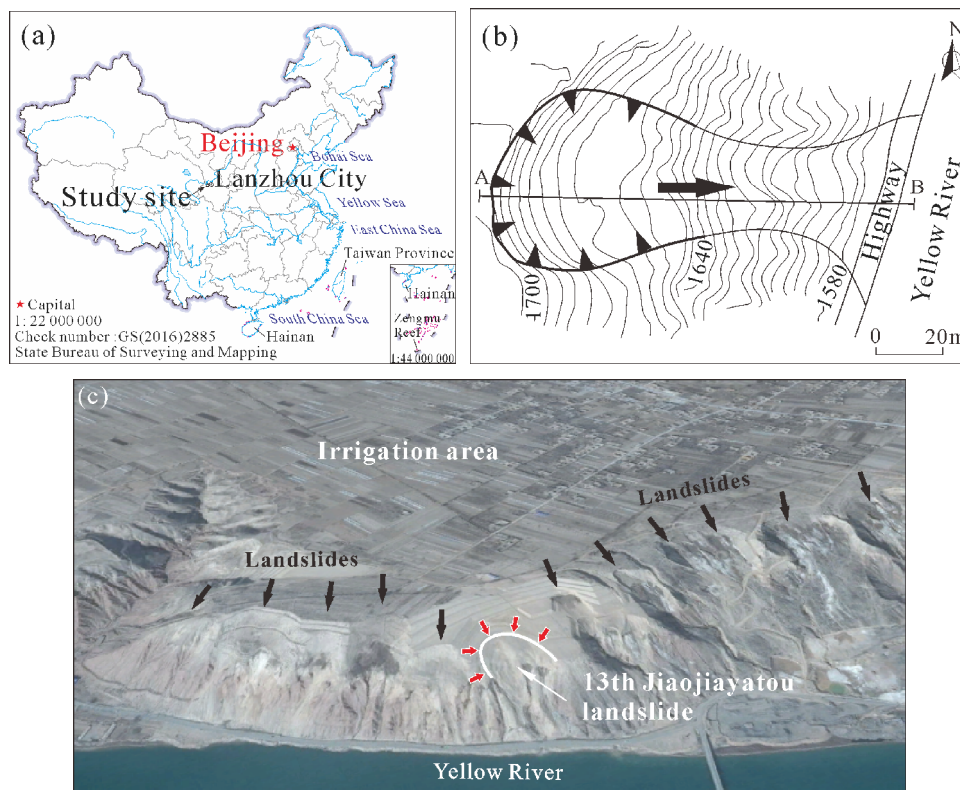
Figure 1 (a) Location of the study area, (b) plan of the study landslide, and (c) the landslides distributing along the Heifangtai platform edge (the base image was reproduced from Google Earth).

et al. 2004), and the groundwater table has risen by approximately 16 m since 1980 (Wang 1997; Derbyshire et al. 2000) (Figure 2c). Springs can commonly be observed at the foot of platform edge slope. The 15 km² platform in Heifangtai is famous for irrigation-induced loess landslides in the world (Derbyshire et al. 2000). More than 120 failures have occurred over the past three decades. From 1977 to 2010, the platform cliff retreated by 126 m. Dense cracks are located around the edge of the platform.

In this area, March and November are the months with largest amount of irrigation (Figure 2b). Large numbers of landslides would occur during and after the period. Irrigation-induced loess landslides occurring after the peak irrigation time indicates time-dependent water infiltration. A new loess landslide, i.e. the 13th Jiaojiayatou landslide occurred on April 27, 2011. This landslide is situated on a steep slope (approximately 45°) on the northeast flank of the Heifangtai platform (location: N 36°05′00″, E 103°18′00″) (Figure 1b, c). It was a flow-like failure with 75 m long and 120 high. Its deposition buried the highway at the foot of the slope, further flowing into the Yellow River

(Figure 1c). The upper layer of the slope is composed of upper Pleistocene loess that is approximately 25 to 60 m thick, and the bedrock is composed of lower Cretaceous mudstone. There is a thin layer of clay overlying the bedrock (Figure 3). Several open tension cracks and steps were observed along the edge of platform after the landslide. The head scarp of the landslide is a cliff showing loess joint fissures.

2 Experimental Methodology

2.1 Used centrifuge facility and materials

The test was conducted using the TLJ-500 geotechnical centrifuge facility at the State Key Laboratory of Geological Hazard Prevention and Geological Environment Protection (SKLGP) in Chengdu University of Technology (CDUT) (Figure 4). The TLJ-500 has an effective radius of 4.5 m and a rectangular rigid soil box with internal dimensions of 100 cm in length, 100 cm in width and 60 cm in height. One of the sides of the box is equipped with transparent lucite material that forms a window to view the soil model during test.
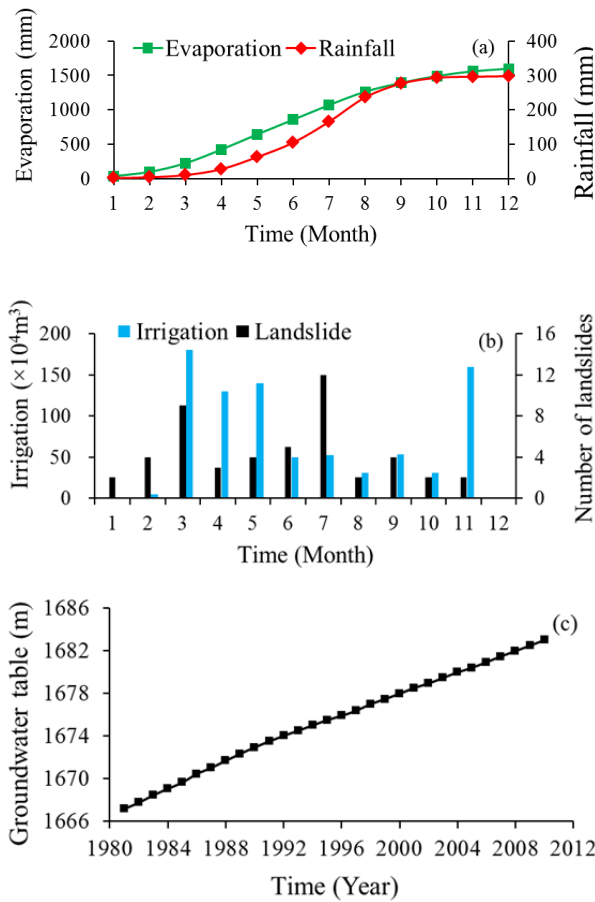
Figure 2 (a) Variation of evaporation and rainfall in each month, (b) irrigation volume and number of landslides in each month, and (c) changes of groundwater table from 1980 to 2009 (landslide data from Wang et al. (2004); irrigation data from Xu et al. (2010)).
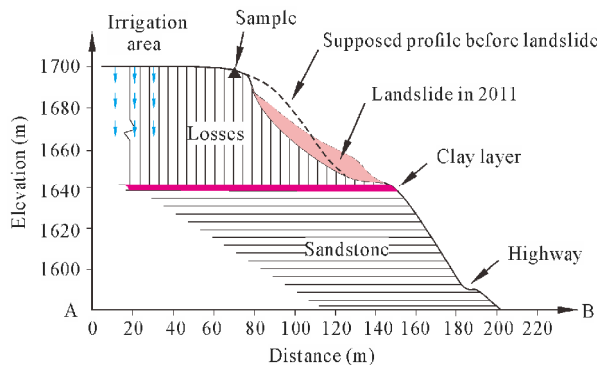

Figure 3 Longitudinal section along the line A-B as shown in Figure1b.

To retain the original structure of the loess, a cubic loess block with 1 m in length of side was taken from the source area of the study landslide. It was carefully carried to laboratory. Figure 5 shows the particle size distribution of the loess material.

The other properties of the loess are summarized in Table 1. Its content of silt particle (<0.075 mm) is more than 80 % with a void ratio of 1.19 and a natural water content of 5.2%.

Figure 4 Photograph of the centrifuge machine.
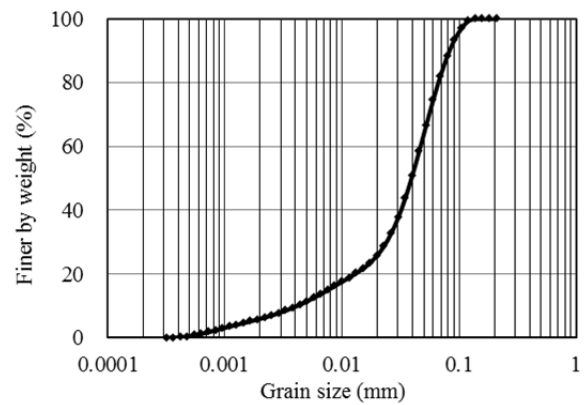
Figure 5 Grain size distribution of the loess sample.

Table 1 Properties of the studied loess

Soil properties	Value
Dry density (kg/m³)	1.45×10^3
Void ratio	1.19
Specific gravity	2.72
Plastic limit (%)	17.0
Liquid limit (%)	24.1
Water content (%)	5.2

2.2 Model construction

If a small scale (*n* times smaller than full scale) model is used in a centrifuge model, according to the centrifuge scaling rule, the model acceleration should be increased by *n* times. In our study, the

maximum acceleration is 200 times gravitational acceleration, i.e., 200 g.

The centrifuge model was constructed in a rigid box. The lower part of the model was modeled using concrete to represent the bedrock (Figure 6). The 2-cm-thick clay layer on the bedrock was modeled using clay obtained from the landslide site. The upper loess layer was constructed using the cubic block. First, the loess block was whittled to a model with outside dimensions of 50 cm × 60 cm × 60 cm, and then the semi-finished model was placed on the clay layer in the model box. It was then whittled into the final slope geometry as shown in Figure 6. The gap (1 cm) between the soil model and the wall of the box was filled with dense dry loess. Waterproof material was painted on the model boundaries as shown in Figure 6.

Figure 6 Model preparation (grid lines, landmarks and isolate water material).

2.3 Measurement systems

The measurement systems included an image-capture system and transducers. The image-capture system included a digital camera and used the Particle Image Velocimetry (PIV) technique. The camera, which had a resolution of 5 megapixels, was installed in front of the window of the model box to record video during the test. The PIV technique was introduced by White et al. (2003) from hydromechanics, and has been widely used to quantify soil displacement behavior in geotechnical engineering (Stanier and White 2013; Cao et al. 2015; Fan et al. 2016). This system consisted of a Charge Coupled Device (CCD) camera, a data collection computer, a control computer and image analysis software. The cross section image of the centrifuge model could be

taken by the CCD camera through the box window. To let the cameras get clear images, bright LED lights were placed in front of the window. Grid lines and landmarks were drawn on the window (Figure 6). And the locations of the landmarks before and after the centrifuge test were recorded by the PIV system, which were used to calculate the displacement victors of the landmarks to obtain the displacement contours in the horizontal and vertical directions.

2 displacement transducers, 6 earth pressure transducers and 6 pore pressure transducers were embedded in the model along two longitudinal sections (Figure 7). The displacement transducers are Linear Variable Differential Transducers (LVDTs) that have a reliable measurement range of ±5 mm. The pore pressure transducers are cylindrical with a diameter of 33 mm and a length of 180 mm. They can measure pore pressures up to 400 kPa at a resolution of 0.2 kPa. The earth
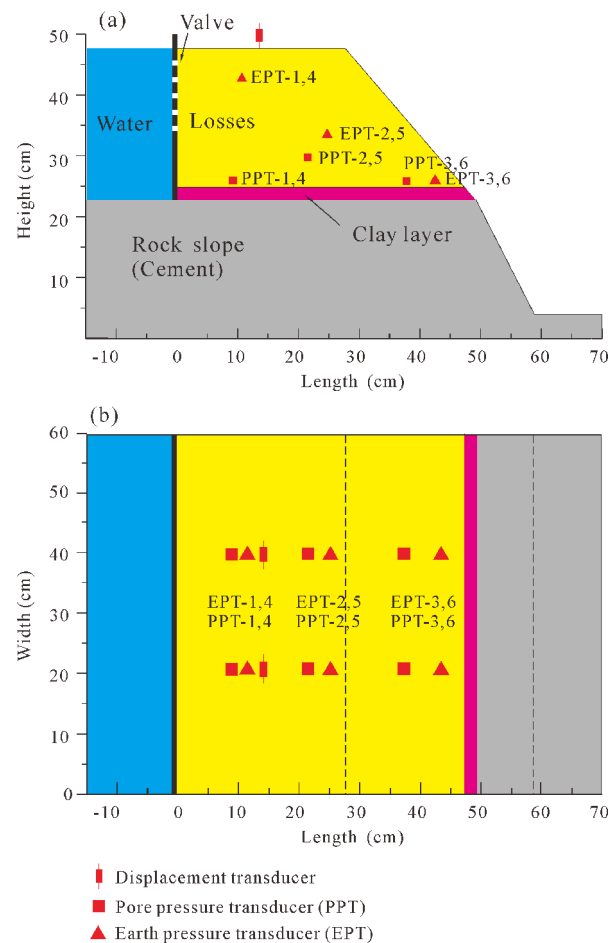

Figure 7 Schematic view of slope model for the centrifuge test. (a) Front view, (b) top view.

pressure sensors are strain gauge type transducers with 30 mm in diameter and 13 mm long. Their reliable maximum earth pressure is 500 kPa.

2.4 Irrigation modeling

In Heifangtai area, the irrigation area was located at the back of the platform (Figure 1c). The irrigation water infiltrated downward and flowed within the basal layer until out at the foot of the edge slope (Xu et al. 2014). To simulate irrigation water infiltration in slope, a tank with 60 cm long, 20 cm wide and 59 cm high was designed and placed at the back of the slope model (Figure 7). Five rows of 2.5-mm-diameter holes were distributed on the front wall of the tank, through which water in the tank could be introduced into the loess slope. These holes could be individually opened or closed by irrigation valves to control the amount of irrigation water.

There was not hydrological process in the model prior to the centrifuge test. All of the irrigation valves were closed firstly, and the centrifuge was spun for 10 min at an acceleration of 10 g to equilibrate the model. After this spinning stage ended, assuming that the steady state of the model was reached, all of the irrigation values were opened after adding water to the tank to a height of 35 cm, and the centrifuge was restarted to an acceleration of 150 g. The 150-g stage was spun stably for 6 min to forming a flow field in the model. And then the acceleration was increased to 200 g. At this stage the model was stably run for 15 min to investigate the failure processes. Finally, the acceleration was decreased gradually to zero to end the test.

3 Test Results

3.1 Deformation and failures

The slope subsided gradually during the centrifuge spinning (Figure 8). The subsidence increased rapidly as the acceleration increased
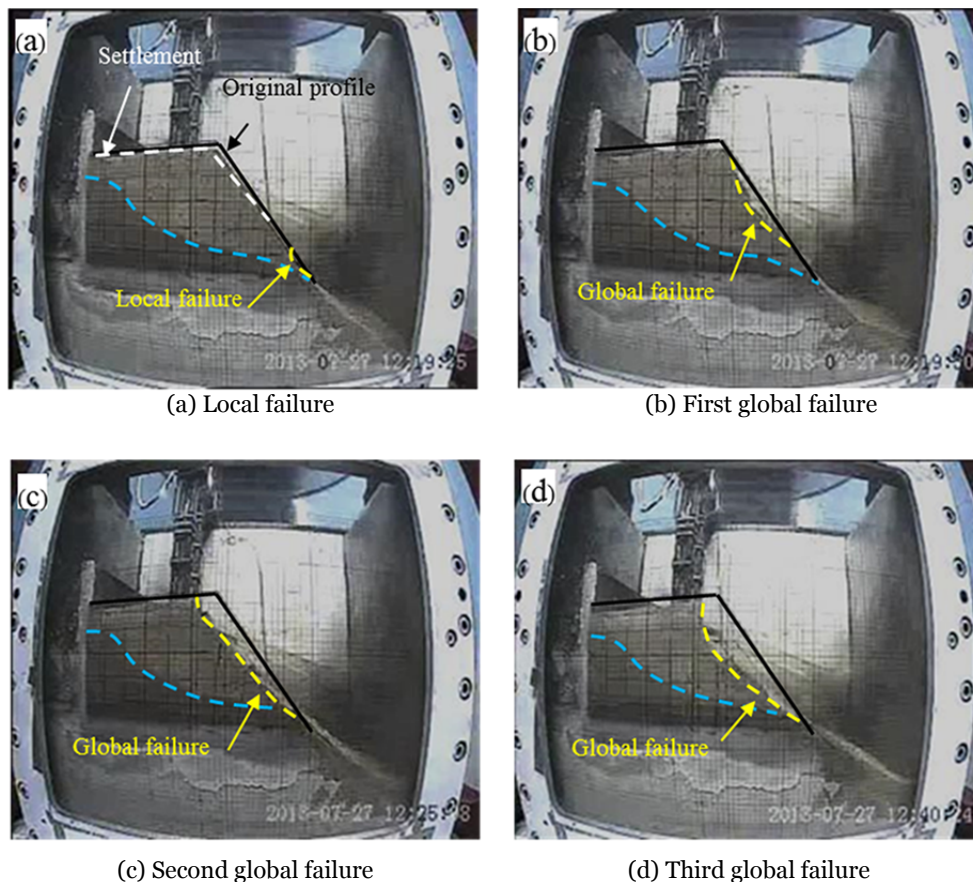

(a) Local failure

(b) First global failure

(c) Second global failure

(d) Third global failure

Figure 8 Photos taken by image-capture system. Time is (a) 987 s, (b) 1045 s, (c) 1407 s, (d) 1681 s respectively.

from approximately 120 g to 150 g. During the 150-g acceleration the subsidence curve converged, which indicated that the model had reached a new equilibrium. The subsidence increased by 3 mm as the acceleration increased from 150 g to 200 g. There was little subsidence after reaching the acceleration of 200 g. The detected total subsidence was approximately 23 mm. The subsidence decreased by approximately 1 mm as the centrifuge was stopped (Figure 11a).

The observed failures were divided into local (shallow) failures and global (large) failures. A local failure was firstly triggered at the foot of the slope at an acceleration of approximately 120 g (Figure 8a). When the 150 g acceleration was reached, a global failure (first large failure) with an arc-shaped sliding surface was occurred in the middle of the slope (Figure 8b). The second global failure was occurred as the acceleration increased from 150 g to 200 g (Figure 8c). This failure was originated at the upper part of the slope and extended to a relatively flat failure surface. This failure caused regressing of the platform edge. During the stage of 200 g, the third global failure was triggered in the source area of the second one. The scarp height of the centrifuge model was largely enlarged due to this failure (Figure 8d). It is worth noting that two of the three global failures were triggered during constant acceleration stages with little subsidence. The other one occurred during the transition from 150 g to 200 g, when only slight subsidence was occurred. This information suggests that irrigation-induced slope failures might be triggered after the slope subsidence.

Cracks and water table in the model during test were detected from the video image. There sketches were drawn as shown in Figure 9. Cracks developed at the foot of the slope firstly where following a local failure. And then, the cracks formed upward. After the first global failure on the middle part of the slope, cracks parallel to the edge of the model developed. It can be found that the open tension cracks formed the boundaries of the second and third failures. The failure processes was characterized by regressive failures. It should be noted that the water table in front of the slope increased prior to each global failure, while the water table in the middle and the back of slope was almost constant (Figure 9).

The markers displacements were calculated in the image analysis subsystem. The results are shown in Figure 10a. The vertical and horizontal displacement contours are shown in Figures 10b and c. The contour lines at the base in both directions are nearly parallel, which indicates a linear distribution of displacement. However, both the vertical and horizontal deformations are concentrated around the water table suggesting non-uniform strain due to possible soil creep.

3.2 Pore pressure

The pore pressure data are shown in Figure 11b. The pore pressures at pore pressure transducers PPT-1 and PPT-4 began to increase after spinning for approximately 200 sec, which indicates arriving of the irrigation water. The pore pressures at PPT-3 and PPT-6, which were located at the foot of the slope, increased rapidly after approximately 800 sec indicating the arrival of irrigation water at the front portion of the slope. During the 150 g, the pore pressures at PPT-1, PPT-4, PPT-2 and PPT-5 decreased firstly and then increased, which indicates the change of pore pressure generation and dissipate. However, the pore pressures at PPT-3 and PPT-6 continued to increase gradually. When the 200 g acceleration was maintained, the pore pressures of all pore pressure transducers decreased. Except the third failure which resulted in a rapid 16-kPa-increase pore pressure at PPT-2 and PPT-5, the pore pressure transducers did not response obviously to the failures. It is because all the failures were triggered above the pore pressure transducers.

3.3 Earth pressure

Two earth pressure transducers (EPT-4 and EPT-5) did not work. Therefore, earth pressure data were obtained from the other four transducers (Figure 11c). The earth pressures at transducers EPT-3 and EPT-6 increased to approximately 110 kPa with increasing acceleration at the beginning of the test, while the earth pressures at transducer EPT-1 (in the upper part of the slope) and EPT-2 (in the middle part) did not change significantly. After that, the pressures at EPT-3 and EPT-6 increased unsteadily, which indicated the occurrence of the local failure at the foot of the
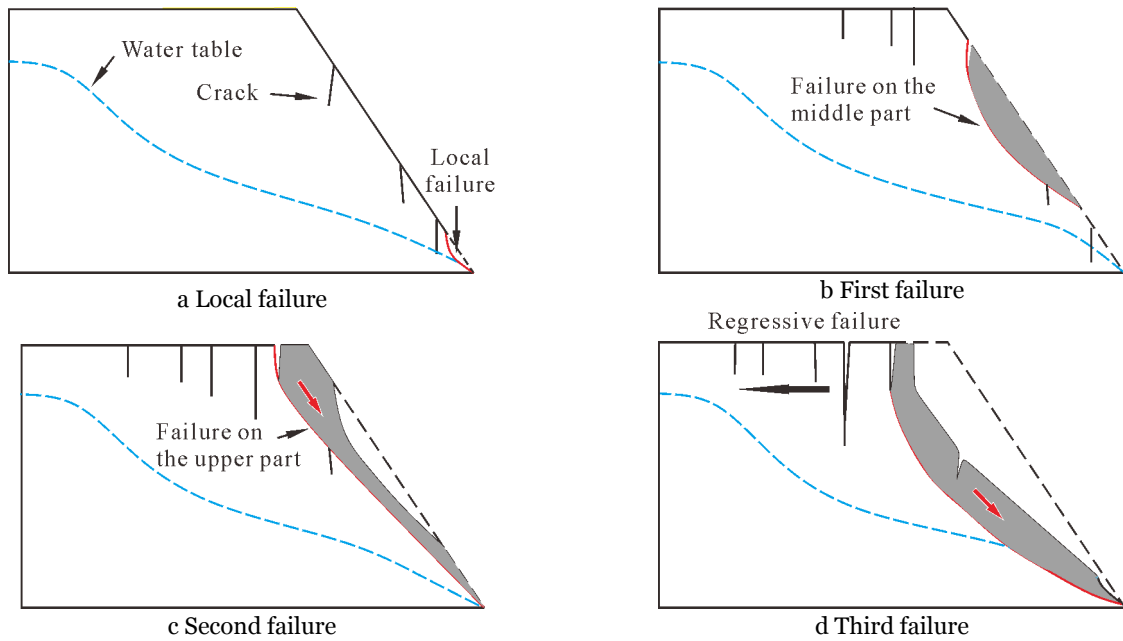
Figure 9 Showing the cracks, failure and water table of the slope at different failure times. (a) Spring was observed at the foot of the slope where a local failure formed. Cracks were starting to develop upward. (b) Cracks extended to the top of the model, and a global failure was occurred at the middle part with increasing water table. (c) Cracks developed backward, and an open tension crack formed the back boundary of a large failure. (d) More open tension cracks developed, and another global failure was triggered with increasing water table. These failure processes had the characteristics of regressive failure.
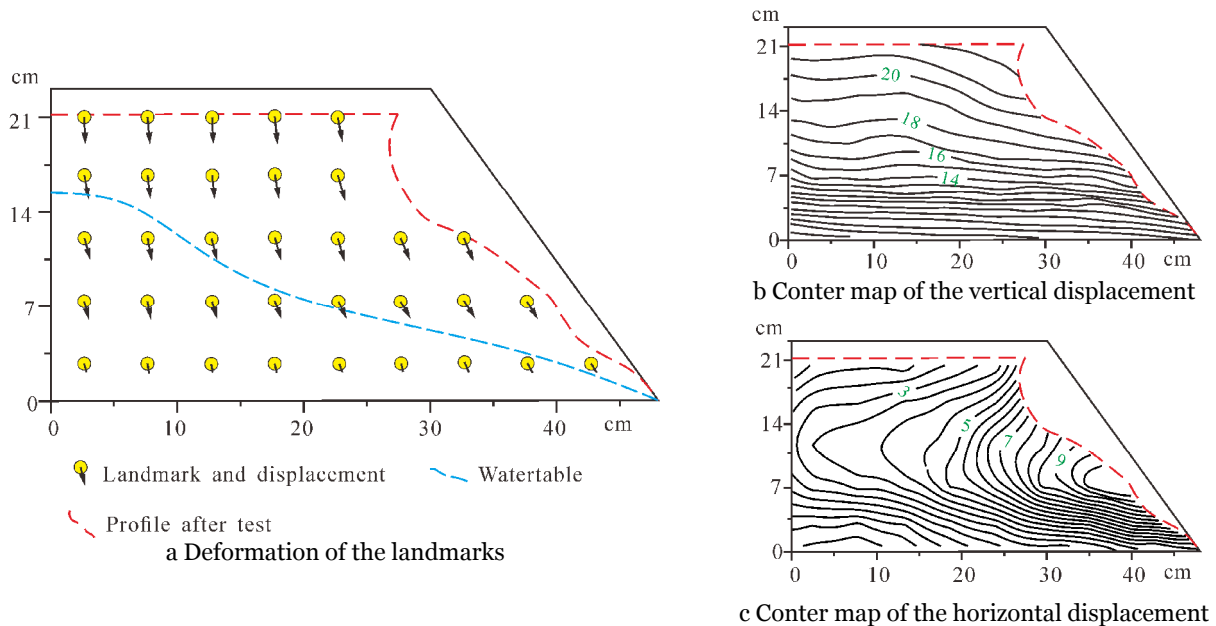

Figure 10 Final deformation of the model.

slope. When the first global failure occurred, EPT-2 had a sudden increase of 48 kPa, but EPT-1 had no response. After the first global failure, the earth pressure at the foot of the slope (EPT-3 and EPT-6) decreased unsteadily until the acceleration increased from 150 g to 200 g. When the second failure occurred, EPT-2 had a rapid increase by approximately 80 kPa. As the 200 g acceleration was maintained, the pressure at EPT-3 continued to increase. It had a rapid increase by approximately 45 kPa due to the third global failure. After the third failure event, the pressure at

EPT-3 decreased abruptly by approximately 125 kPa. When acceleration decreasing, the earth pressures decreased at all of the transducers. It is important to note that EPT-3 and EPT-6 were shallow embedded at the foot of the slope, but very high earth pressures were recorded by them. And they responded to all failures during test.

4 Discussion

Loess is characterized by well-developed vertical joints and macroporous structure, and susceptibility to collapse during wetting, resulting that loess is vulnerable to water, such as rainfall and irrigation. Generally, rainfall-induced failures are characterized by relatively shallow failure on deposit covering slopes (Cascini et al. 2014). Their displacements maybe essentially controlled by their seasonal fluctuations, i.e., wet season with highest rate of displacement and progressive reduction as the dry season approaches. And the seasonal effects may be connected to rainfall patterns, such as frontal rainfall, hurricane-like rainfall or isolated convective storms (Cascini et al. 2014). While, irrigation-induced failures are affected by human agricultural activities. Rather than rainfall which is a transient even general from minutes to days, irrigation duration can be as long as several months per year (Wang et al. 2004).

The behavior of both rainfall-induced failure and irrigation-induced failure are hydro-mechanical processes, and their soil strain behaviors are related to effective stress with starting wetting stage (Cuomo et al. 2017), but there is distinct difference between them. During rainfall, water infiltrates downward in slope. Slope instability depends on wetting band accompanied by a decrease in matric suction. The magnitude of rainfall-induced wetting front suction plays a key role in the stability, and the factor of safety dropped rapidly once the critical wetting band depth reached (Kim et al. 2004). In our case, although the irrigation area is located at the back of the platform, water fluxes along the basal layer, and comes out at foot of platform edge slope following by rising of the water table. This study showed that irrigation-induced slide started by local failures (Figure 9) with transient localized excess pore-water pressures (Figure 11) due to local

variation of the hydraulic conditions in base layer. Although Sorbino and Nicotera (2013) proposed that reducing matric suction in unsaturated soils due to infiltration may be predisposes to slope failure, our study shows that the localized excess pore-water pressures is primary for attaining slope failure.

Although both the acceleration level and water content changed during our centrifuge test, the two failures were triggered with g-levels smaller than the goal value. And the other two global failures occurred at the stable g-level, i.e., 150 g-level and 200 g-level. These evidences show that the influence of the change of g-level could be eliminated during out centrifuge test. It can be reasonable inferred that these landslides were mainly induced by the irrigation. Unlike rainfall-induced loess landslides, which are characterized by sudden global failures (Ling et al. 2012), or excavation-induced loess landslides, which will be stable until reaching a critical excavation angle or height at the slope toe (Fan et al. 2016). This centrifuge model test shows that local failure at the toe of slope is first triggered (I). And then larger slide is triggered in the middle part of slope (II). After that, the upper part of slope can be detached from source area (III). It follows a flow-like shear failure along the entire slope leaving a deep concave topography (IV). These processes are characterized by regressive landslides. Data from the Geological Survey Center in Xian (Not published) shows that the studied slope was once failed in May, 2010. Two cracks with 3 cm in wide were observed in the middle of the slope after that failure. And springs were observed at the foot of the slope. A following global failure occurred in April 4, 2011, just 23 days before our case (the 13th Jiaojiayatou landslide). These site evidences showed that the 13th Jiaojiayatou landslide was a regressive landslide similar to the observation in our centrifuge test.

During the centrifuge model test, open tension cracks generated from bottom to up before slope failures and then they formed the boundaries of the following landslides, such as in steps III and IV. Xu et al. (2012) studied the cracks in site near the edge of irrigated loess platforms in Northeast China. They classified them as shallow and deeply penetrating cracks, which control the inflow of irrigation water. Thus, it is important to consider the

effects of cracks under the combination of irrigation and precipitation in the stability studies of irrigation-induced loess landslides. After our test, cracks were widely developed along the edge of the model. In site, a lot of open tension cracks and steps were observed at the edge of platform. The head scarp of our case is a cliff showing loess joint fissures (Figure 12). Although our centrifuge model

is much smaller than the case, these features are similar to the site, which indicates that centrifuge model test is a useful method for studying irrigation-induced loess landslides and that our test results are reasonable.

Figure 13 shows the earth pressure value at each failure time of EPT-1, EPT-2 and EPT-3 respectively. It can be found that the earth pressure
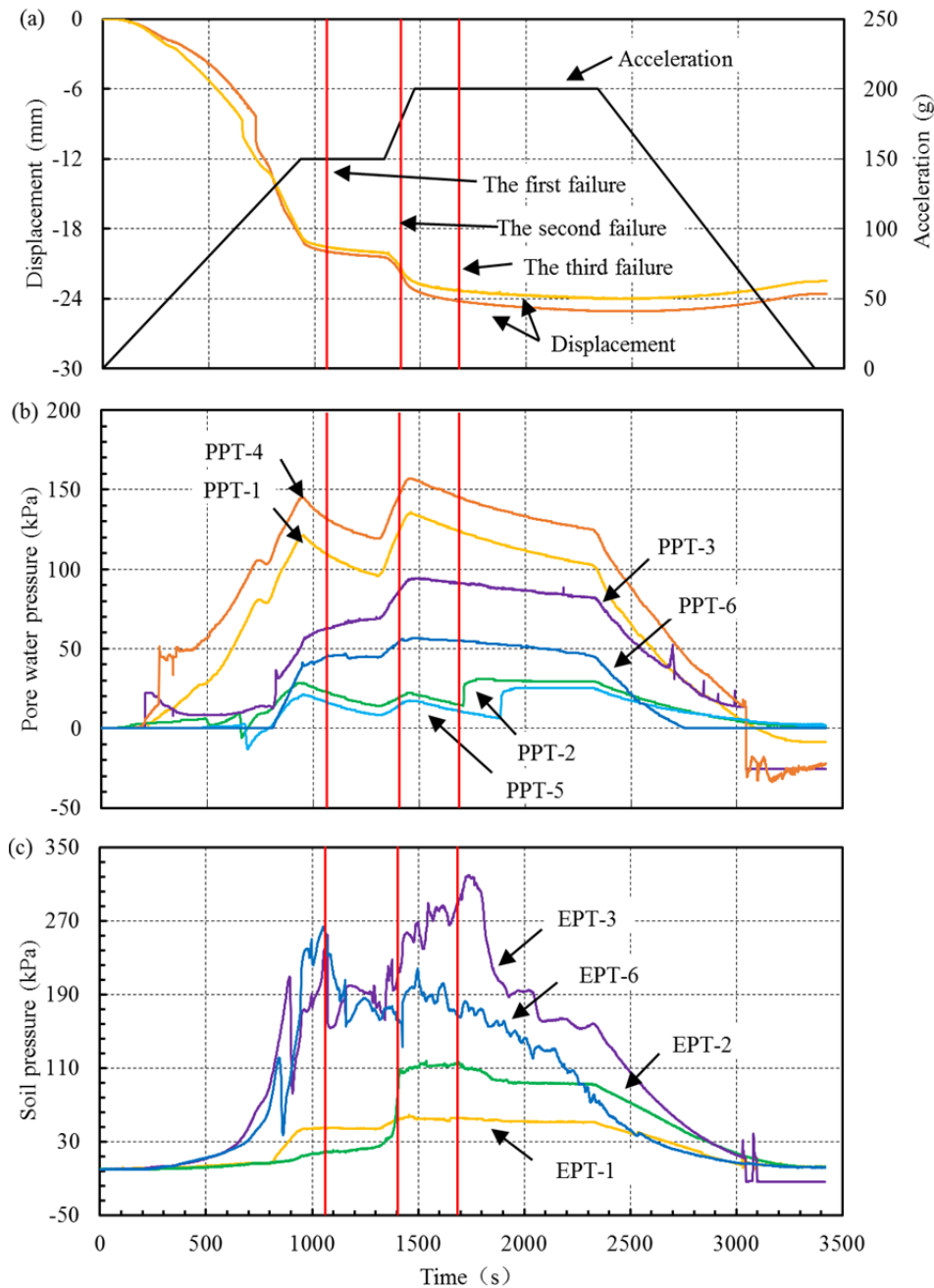

Figure 11 Time series data of centrifuge test. (a) Control signal for acceleration of model and measured displacement, (b) measured pore pressure and (c) earth pressure.

at the foot of slope is the highest suggesting an area of stress concentration before failure. It should be noted that additional earth pressure should be applied to the lower part of the model during centrifuge test. The cause of pressure concentration may be creeping of upper part. After slope failure, the earth pressure decreased immediately until the next failure. Figure 14c shows that the pore pressure at the foot of the slope (PPT-3 and PPT-6) increases with increasing earth pressure, but this feature is not be found at the other two locations (Figures 14a and b). In addition, Figure 11b shows that the pore pressures of PPT-1 and PPT-4 decrease around the first global failure even, while PPT-3 and PPT-6 increase consistently, PPT-2 and PPT-5 were almost constant. These evidences suggest that water might be accumulated at the foot of slope due to the local variation of the hydraulic conditions in base layer. There might be
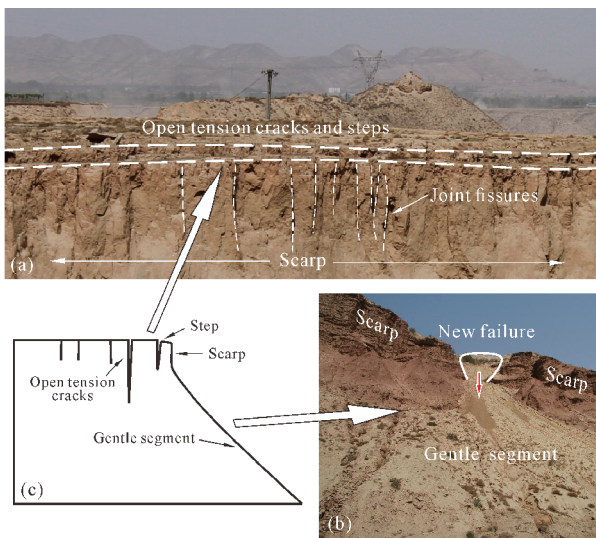

Figure 12 Comparison of slope failure model between field case and test result. (a) Scarp and (b) failure profile of the field case, (c) slope failure model of centrifuge test result.
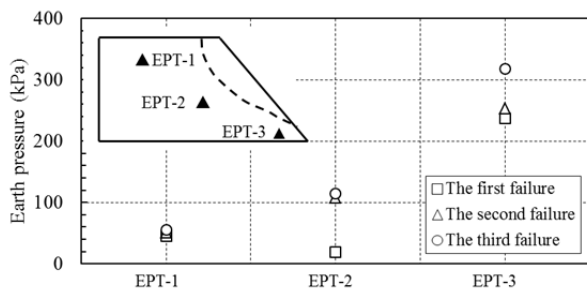

Figure 13 Earth pressure data of EPT-1, EPT-2 and EPT-3 at each failure time. The earth pressure at the foot of slope is the highest, suggesting that there is a stress concentration area before each failure.

a critical pore water pressure for slope failure, which should be considered for hazard prevention. Thus, for irrigation-induced loess landslide, the foot part of slope is very important for slope instability and hazard prevention. Investigations of pore-water and earth pressures may be useful for their predicting and early warning.

As shown by our centrifuge test, the failures mainly occurred in unsaturated part of the model, suggesting that matric suction of soil is important for slope stability. The relationship between the study soil suction and water content was investigated (Figure 15). The result shows that the matric suction decreased rapidly with increasing water content. With water content increasing from 9 % to 34 %, the suction decreased from 120 kPa to 7 kPa. The suction decreased rapidly to almost zero with further increasing water content. In a loess slope, there should be an unsaturated zone above water table. Due to suction decreasing, creeping occurs in the unsaturated zone. The vertical and horizontal creeping deformations in the unsaturated zone may be responsible for the slope failure above water table and the cracks on slope and along edge of platform. Cascini et al. (2010) outlined the existence of slide, flow-like slide, and slide to flow. Slide is a slope failure occurring under pore-water drained conditions, while a flow-like slide occurs under partially or totally undrained conditions. And flow-like slides are associated with increase of pore-water pressures. Their classification was consistent with our study. The first and second failures in our test were slide events in unsaturated zone.

To further investigate property of the unsaturated soil, modified Coulomb failure criterion was used for partially saturated soil according to the previous studies (Ling et al. 2009; Ling et al. 2012),

$$\tau_f = c^* + \sigma_n{'} \tan\varphi$$

where τ_f is peak shear strength, and c^*, $\sigma_n{'}$ and φ are apparent cohesion, effective normal stress and angle of internal friction, respectively. If total normal stress (σ_n) is constant and pore pressure (u) increases, the effective normal stress ($\sigma_n{'} = \sigma_n - u$) would decreases. Therefore, the higher the pore pressure, the lower the shear strength (Zhang et al. 2013). To validate this concept of the study loess with wetting, a series of direct shear tests were conducted on the undisturbed loess samples that
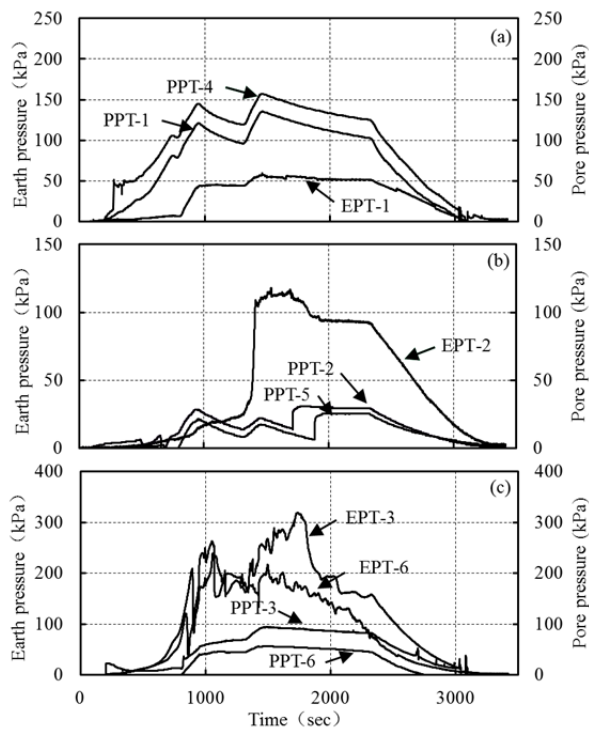
Figure 14 Time series data of earth pressure (EPT) and pore pressure (PPT). (a) PPT-1, PPT-4 and EPT-1. (b) PPT-2, PPT-5 and EPT-2. (c) PPT-3, PPT-6, EPT-3 and EPT-6.
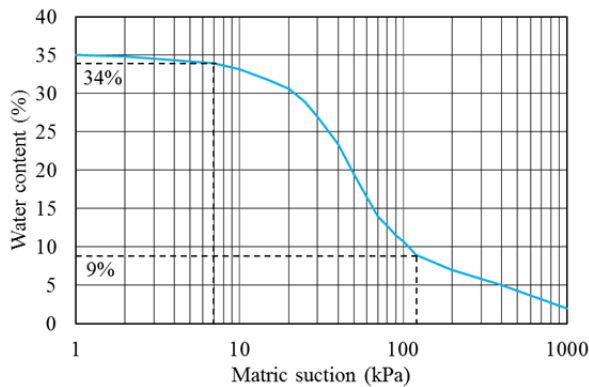

Figure 15 Relationship between the matric suction and water content of the studied soil.

were identical to the centrifuge model soil. The tests were conducted on the specimens with different moisture contents, including 5%, 15%, 25%, and 35%. The results of peak shear strength were shown in Figure 16a. It shows that the soil at the 5% moisture content have an apparent cohesion of 34.9 kPa and an internal friction angle of 30.7° (Figure 16a). However, the apparent cohesion and internal friction angle decrease to 18.1 kPa and 15.1°, respectively when the moisture

content increases to 35%. After the centrifuge test, three samples (S-1, S-2 and S-3) under wetting front were collected to test their properties ((Figure 16c). Their water contents ranged from 20.4% to 20.7%. The apparent cohesion and internal friction angle of S-1 were 16.8 kPa and 14.7°, respectively, which almost equal to the residual strength parameters of the undisturbed loess under same water content condition (Figure 16b). Its void ratio is only 0.89. However, the strength parameters of S-2 (19.7 kPa and 19.1°) and S-3 (21.8 kPa and 21.2°) trended to the peak strength parameters of
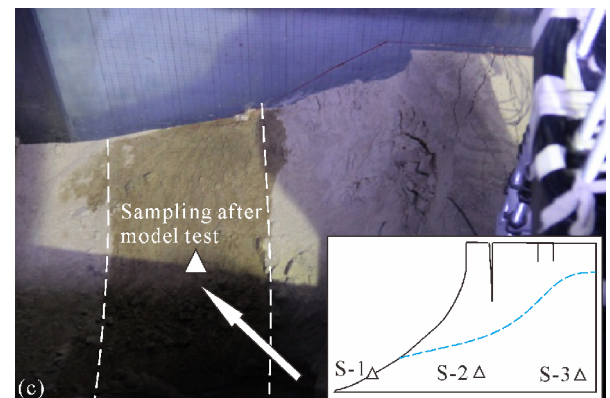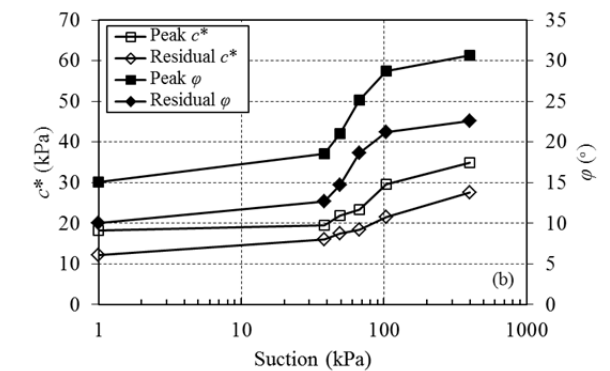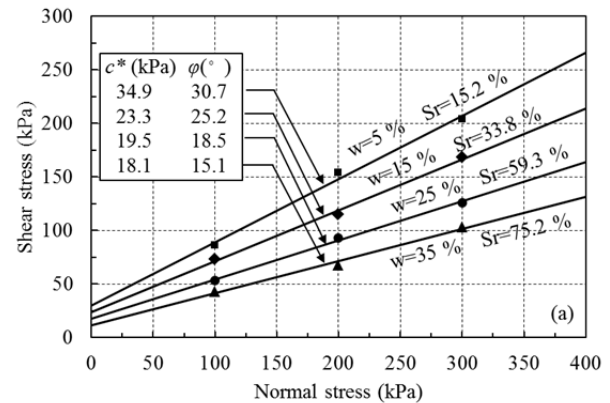

Figure 16 (a) Effects of moisture content on direct shear strength of soil, (b) relationships between suction and shear strength parameters, and (c) sample locations after centrifuge test.

the undisturbed loess. And their void ratios increase to 1.05 and 1.12, respectively. It is reasonable to infer that the irrigation water in the slope changed not only the effective stress but also the structure of the loess. The creep and structure collapse of the loess reduced its void ratio that may result in water table uplift. The increase of water table, time dependent collapse of soil structure and creep may trigger static liquefaction in the basal layer of loess slope. They were responsible for the instability of loess slope.

5 Conclusion

A centrifuge model test was conducted to investigate the behavior of a loess slope under irrigation condition. The variations of pore pressure and earth pressure in the model were measured during the test. The deformation characteristics and failure processes were analyzed using an image measurement system. The irrigation-induced failures of the model and the influence of water content were discussed. The following conclusions can be drawn from this study.

(1) Irrigation-induced failures of loess slopes are characterized by regressive landslides. Failure first occurred at toe of slope, and then in the middle part. The upper part then detached as a fall which triggered following flow-like failure.

(2) Cracks were widely developed around edge

of loess platform during slope failure process. These open tension cracks were parallel to the platform edge.

(3) The foot part of slope is very important for slope instability and hazard prevention in the study area, where concentration of earth pressure and generation of high pore-water pressures would form before failures. The measurements of earth pressure and pore-water pressure might be effective for early warning in the study area.

(4) Shear strength testing of the undisturbed loess showed that an increase of the water content caused reductions of both apparent cohesion and angle of internal friction. The creep and structure collapse of the soil reduced the loess void ratio that may result in water table uplift in the loess slope. Static liquefaction in the basal layer of loess slope causing by the increase of water table, time dependent collapse of soil structure and creep was responsible for the instability of loess slope.

Acknowledgement

References

Cao ZH, Liu HL, Kong GQ, et al. (2015) Physical modelling of pipe piles under oblique pullout loads using transparent soil and particle image velocimetry. Journal of Central South University 22(11): 4329-4336. https://doi.org/10.1007/s11771-015-2981-0

Cascini L, Cuomo S, Pastor M, et al. (2013) Modelling the post-failure stage of rainfall-induced landslides of the flow type. Canadian Geotechnical Journal 50(9): 924-934. https://doi.org/10.1139/cgj-2012-0375

Cascini L, Sorbino G, Cuomo S, et al. (2014) Seasonal effects of rainfall on the shallow pyroclastic deposits of the campania region (southern italy). Landslides 11(5): 779-792. https://doi.org/10.1007/s10346-013-0395-3

Crosta GB, Prisco CD (1999) On slope instability induced by seepage erosion. Canadian Geotechnical Journal 36 (6):1056-1073. https://doi.org/10.1139/t99-062

Cuomo S, Moscariello M, Foresta V (2017) Wetting tests of partially saturated soils under simple shear conditions. Géotechnique Letters 7(2): 197-203. https://doi.org/10.1680/jgele.17.00019

Derbyshire E, Wang JT, Jin Z, et al. (1991) Landslides in the Gansu Loess of China. Catena, Cremlingen, Supplement 20: 119-145.

Derbyshire E, Wang JT, Billard A, et al. (1991). Landslides in the Gansu loess of China. In: Okuda S, Rapp A, Zhang L (eds), Loess: Geomorphological Hazards and Processes. Catena Suppl., vol. 20, pp 119–145.

Derbyshire E, Dijkstra TA, Smalley IJ, et al. (1994) Failure mechanisms in loess and the effects of moisture content changes on remolded strength. Quaternary International 24:5-15.

Derbyshire E, Meng XM, Dijkstra TA. (2000) Landslides in the Thick Loess Terrain of North-West China. Wiley, Chichester. pp 1-256.

Eckersley D (1990) Instrumented laboratory flowslides. Geotechnique 40(3): 489-502. https://doi.org/10.1680/geot.1990.40.3.489

Fan ZJ, Kulatilake PHSW, Peng JB, et al. (2016) In-flight excavation of a loess slope in a centrifuge model test. Geotechnical and Geological Engineering 34(5):1-15. https://doi.org/10.1007/s10706-016-0067-x

Gattinoni P, Francani V (2009) A tool for modeling slope instability triggered by piping. World Academy of Science Engineering and Technology 3 (8):238-244.

Kim J, Jeong S, Park S, et al. (2004) Influence of rainfall-induced wetting on the stability of slopes in weathered soils. Engineering Geology 75(3): 251-262. https://doi.org/10.1016/j.enggeo.2004.06.017

Lee YS, Cheuk CY, Boltonbolton MD (2008) Instability caused by a seepage impediment in layered fill slopes. Canadian Geotechnical Journal 45(10): 1410-1425. https://doi.org/10.1139/T08-067

Lei XY (1995) The hazards of loess landslides in the southern tableland of Jingyang County, Shaanxi and their relationship with the channel water into fields. Journal of Engineering Geology 3(1): 56-64. (In Chinese with English abstract)

Lei XY (2001) Geo-hazards in loess plateau and human activity. Science Press, Beijing, pp 258-264 (In Chinese).

Li TL, Long JH, Li XS (2007) Types of loess landslides and methods for their movement forecast. Journal of Engineering Geology 15(4):500-506. (In Chinese)

Lin ZG, Wang SJ (1988) Collapsibility and deformation characteristics of deep-seated loess in China. Engineering Geology 25(2-4):271-282. https://doi.org/10.1016/0013-7952(88)90032-4

Ling H, Ling HI (2012) Centrifuge model simulations of rainfall-induced slope instability. Journal of Geotechnical and Geoenvironmental Engineering 138(9): 1151-1157. https://doi.org/10.1061/(ASCE)GT.1943-5606.0000679

Ling HI, Wu MH, Leshchinsky D, et al. (2009) Centrifuge modeling of slope instability. Journal of Geotechnical and Geoenvironmental Engineering 135(6): 758-767. https://doi.org/10.1061/ASCEGT.1943-5606.0000024

Liu TS (1985) Loess and environment. China Ocean Press, Beijing. (In Chinese)

Meng XM, Derbyshire E (1998) Landslides and their control in the Chinese Loess Plateau: models and case studies from Gansu Province, China. Geol Soc Lond Eng Geol Spec Publ 15(1):141-153. https://doi.org/10.1144/GSL.ENG.1998.015.01.15

Moriwaki H, Inokuchi T, Hattanji T, et al. (2004) Failure processes in a full-scale landslide experiment using a rainfall simulator. Landslides 1(4): 277-288. https://doi.org/10.1007/s10346-004-0034-0

Schofield AN (1980) Cambridge geotechnical centrifuge operations. Geotechnique 30(3):227-268. https://doi.org/10.1680/geot.1980.30.3.227

Sorbino G, Nicotera MV (2013) Unsaturated soil mechanics in rainfall-induced flow landslides. Engineering Geology 165: 105-132. https://doi.org/10.1016/j.enggeo.2012.10.008

Stanier SA, White DJ (2013) Improved image-based deformation measurement in the centrifuge environment. Geotechnical Testing Journal 36(6):1-14. https://doi.org/10.1520/GTJ20130044

Tamrakar SB, Toyosawa Y, Itoh K, et al. (2006) Failure heights comparison during excavation using in-flight excavator. In: Ng CWW, Zhang LM, Wang YH (eds) Physical modelling in geotechnics. Taylor & Francis Group, London. pp 385-390. https://doi.org/10.1201/NOE0415415866.ch52

Take WA, Bolton MD (2002) A new device for the measurement of negative pore water pressures in centrifuge models. Reproductive Biology 13 (Suppl 2):25-26.

Take WA, Bolton MD, Wong PCP, et al. (2004) Evaluation of landslide triggering mechanisms in model fill slopes. Landslides 1(3):173-184. https://doi.org/10.1007/s10346-004-0025-1

Thusyanthan NI, Madabhushi SPG, Singh S (2007) Tension in geomembranes on landfill slopes under static and earthquake loading-centrifuge study. Geotextiles and Geomembranes 25(2):78-95. https://doi.org/10.1016/j.geotexmem.2006.07.002

Toyosawa Y, Horii N, Tarnate S, et al. (1996) Failure characteristics of a sheet pile wall in centrifuge tests. In: Mair ERJ, Taylor RN (eds) Proceedings of the International Symposium on Geotechnical Aspects of Underground Construction in Soft Ground, London. pp 225-230.

Viswanadham BVS, Rajesh S (2009) Centrifuge model tests on clay based engineered barriers subjected to differential settlements. Applied Clay Science 42(3-4): 460-472. https://doi.org/10.1016/j.clay.2008.06.002

Wakeman, TH, Dunlop P, Knutson L (1997) Current status and future management of dredging at the port authority of New York and New Jersey. In: Meegoda JN, Wakeman TH, Arulmoli A, et al. (eds.), Dredging and Management of Dredged Material: Geotechnical Special Publication 65. American Society of Civil Engineers, Reston. pp 12-22.

Wang GX (1992) Relationship between the origin of loess landslides and the human activities in China. Sixth International Symposium on Landslides. Landslides, vol.1. Balkema. pp 263-268.

Wang JD, Wang JT, Huang HG (1993) A study on creeping or sliding liquefaction of saturated soil. Geoscience (1):102-108 (In Chinese with English abstract).

Wang NQ (1997) Characteristics of landslides caused by irrigation on the margin of loess platform. Journal of Gansu Science 36(Suppl): 103-108. (In Chinese)

Wang ZR, Wu WJ, Zhou ZQ (2004) Landslide induced by over-irrigation in loess platform areas in Gansu Province. Chinese Journal of Geological Hazard and Control 15(3):43-46. (In Chinese with English abstract)

Wang R, Zhang G, Zhang JM (2010) Centrifuge modelling of clay slope with montmorillonite weak layer under rainfall conditions. Applied Clay Science 50(3): 386-394. https://doi.org/10.1016/j.clay.2010.09.002

Wang LP, Zhang GA (2014) Centrifuge model test study on pile reinforcement behavior of cohesive soil slopes under earthquake conditions. Landslides 11(2): 213-223. https://doi.org/10.1007/s10346-013-0388-2

White DJ, Take WA，Bolton MD (2003) Soil deformation measurement using particle image velocimetry (PIV) and photogrammetry. Geotechnique 53(7): 619-631. https://doi.org/10.1680/geot.2003.53.7.619

Xu L, Dai FC, Kwong AKL, et al. (2009) Characteristics and forming mechanisms of the platform-edge cracks and their significance to loess landslide. Geological Review 55(1): 55-59. (In Chinese with English abstract)

Xu L, Dai FC, Min H, et al. (2010) Loess landslide types and topographic features at south Jingyang platform, China. Earth Science - Journal of China University of Geosciences 35(1):155-160. (In Chinese with English abstract)

Xu L, Dai FC, Tham LG, et al. (2011) Field testing of irrigation effects on the stability of a cliff edge in loess, north-west China. Engineering Geology 120(1-4): 10-17. https://doi.org/10.1016/j.enggeo.2011.03.007

Xu L, Dai FC, Gong QM, et al. (2012) Irrigation-induced loess flow failure in Heifangtai Platform, north-west China. Environmental Earth Sciences 66(6): 1707-1713. https://doi.org/10.1007/s12665-011-0950-y

Xu L, Dai FC, Tu XB, et al. (2014) Landslides in a loess platform, north-west China. Landslides 11(6):993-1005.https://doi.org/10.1007/s10346-013-0445-x

Xue Q, Zhang MS, Tang YM, et al. (2011) Deformation analysis of the Jiaojia landslide at Heifang platform based on DEM. Hydrogeology & Engineering Geology 38 (1):133-138. (In Chinese with English abstract)

Yu YZ, Deng LJ, Sun X et al. (2008) Centrifuge modeling of a dry sandy slope response to earthquake loading. Bulletin of Earthquake Engineering 6(3): 447-461. https://doi.org/10.1007/s10518-008-9070-9

Zhang DX, Wang GH, Lou CY et al. (2009) A rapid loess flow slide triggered by irrigation in China. Landslides 6(1): 55-60. https://doi.org/10.1007/s10346-008-0135-2

Zhang FY, Wang GH, Kamai T, et al. (2013) Undrained shear behavior of loess saturated with different concentrations of sodium chloride solution. Engineering Geology 155(6): 69-79. https://doi.org/10.1016/j.enggeo.2012.12.018

Zhang Z, Wang T, Wu S, et al. (2016) Seismic performance of loess-mudstone slope by centrifuge tests. Bulletin of Engineering Geology and the Environment 76(2): 671-679. https://doi.org/10.1007/s10064-015-0846